strongly apparent when the material is changed by stress to a 2-valley or a 1-valley semiconductor. In contrast to the case of Sb donors the mobilities of As-doped Ge have a simple power law dependence on concentration in the range $N>10^{18}$ cm$^{-3}$. They cannot be described by a simple scattering model, however. The presence of an anomalous contribution to the magnetoresistance at these high As concentrations also shows the inadequacy of the simple degenerate model.

The mobility anisotropy factor in As-doped germanium was found to be $K(4)=4\pm0.4$, $K(2)=5\pm0.6$, and $K(1)=6\pm0.5$ for the 4-, 2-, and 1-valley case, respectively. The value $K(2)$ seems to increase and $K(1)$ to decrease slightly as $N$ increases from $10^{18}$ to $10^{19}$ cm$^{-3}$.

In contrast to the case of Sb donors the piezoresistance of degenerate As-doped germanium decreases beyond the theoretical saturation stress and approaches a constant value only at very high stresses. This indicates that the presence of localized tail states and their interaction with the valley or valleys shifted downwards by stress is more strongly pronounced in As-doped germanium.

The mobility ratio $\mu_{11}(\mathrm{Sb})/\mu_{11}(\mathrm{As})$ is found to be larger for the 1 valley case than for the 4-valley case. This indicates that simple intervalley scattering as discussed earlier[8] cannot be the primary reason for the lower mobility of As-doped germanium. It is possible, however, that the resonance scattering to the tail states of the valleys which are moved up by the stress is stronger than intervalley scattering among 4 degenerate valleys. Both of these scattering processes are expected to be less for Sb than for As donors because of the large difference in their central cell potentials.

## ACKNOWLEDGMENTS

It is a pleasure to acknowledge the help of the technical staff of the Low Temperature Laboratory of the University of Chicago who made the cryogenic equipment available to us, and the general support of the Low Temperature Laboratory by the National Science Foundation.

PHYSICAL REVIEW VOLUME 139, NUMBER 5A 30 AUGUST 1965

# Behavior of Coherent Microwave Phonons at Low Temperatures in $Al_2O_3$ Using Vapor-Deposited Thin-Film Piezoelectric Transducers*

J. DE KLERK
*Westinghouse Research Laboratories, Pittsburgh, Pennsylvania*
(Received 19 March 1965)

The intrinsic attenuation and velocity of compressional and shear waves have been measured in a single crystal of $Al_2O_3$ at 1 Gc/sec for $a$-axis propagation. While the slow-shear-mode attenuation shows a $T^4$ temperature dependence as predicted by the Landau-Rumer theory, the fast shear mode has a $T^7$ dependence below 50°K and a $T^4$ dependence at higher temperatures. The compressional mode has a $T^9$ dependence below 50°K and a $T^4$ dependence above this temperature. A theory for this behavior is proposed. The measured 300°K velocities are $v_L=11.03\times10^5$, $v_{T_1}=6.78\times10^5$, and $v_{T_2}=5.72\times10^5$ cm/sec. The three plane-wave modes were generated and detected by a single pair of ZnS vapor-deposited thin-film piezoelectric transducers. The crystallographic orientation of the ZnS films relative to the $Al_2O_3$ was determined by means of reflection electron diffraction and x-ray diffraction. The piezoelectric matrix for ZnS is used to show how independent generation of the three modes was achieved.

## INTRODUCTION

THE behavior of the acoustic attenuation in $Al_2O_3$ at microwave frequencies has been studied by others[1,2] in an attempt to determine the phonon processes involved. In both cases propagation was directed along the $X_3$ or $c$ axis, which only supports one pure acoustic mode,[3] viz., compressional. During the investigation reported here, the acoustic energy was propagated along an $X_1$ axis. Three pure modes can be propagated along such an axis. Such propagation has been achieved, as reported here, using a single pair of vapor-deposited piezoelectric transducers. Thus, for the first time, it has been possible to determine the intrinsic attenuation behavior of all three pure modes along the same axis and on the same specimen. This enables us to make a valid comparison of the attenuation-temperature characteristics of the three modes as propagation conditions were identical for all three modes.

## SAMPLE PREPARATION

Several oriented single-crystal $Al_2O_3$ rods, 1 in. long by 0.25 in. diameter, were obtained from Linde Com-

* The research reported in this paper was sponsored by the U. S. Air Force Cambridge Research Laboratories, Office of Aerospace Research under Contact No. AF 19(628)-4372.

[1] I. S. Ciccarello and K. Dransfeld, Phys. Rev. **134**, A1517 (1964).

[2] T. M. Fitzgerald, B. B. Chick, and R. Truell, J. Appl. Phys. **35**, 2647 (1964).

[3] G. F. Farnell, Can. J. Phys. **39**, 65 (1961).

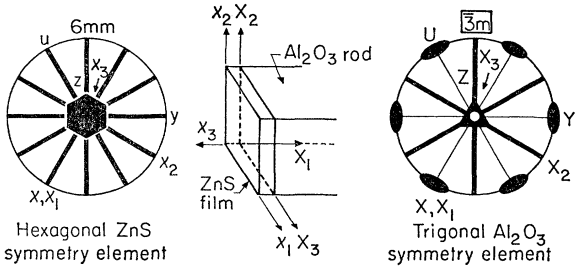


FIG. 1. Orientation of ZnS films relative to the $Al_2O_3$-rod orientation.

pany. The rod axes were supplied parallel to an $a$ axis within 0.2°. The end faces were ground and polished in this laboratory to the following specifications: perpendicularity of the end surfaces to the cylincrical surfaces within ±1 min of arc, flatness within $\lambda/10$ of sodium light, and parallelism within ±2 sec of arc. The cylindrical surfaces were left in the fine-ground condition as received. The sample designated Linde No. 8, which exhibited the lowest acoustic attenuation, was chosen for the measurements reported here.

Thin-film[4] piezoelectric transducers were used for phonon generation and detection. These transducers were vapor-deposited[5] as highly oriented insulating zinc sulfide films.

## TRANSDUCER/SAMPLE CRYSTALLOGRAPHIC ORIENTATION

X-ray-diffraction and reflection-electron-diffraction techniques were used for determining the crystallographic orientations of the $Al_2O_3$ sample and the ZnS film, respectively. Figure 1 shows schematically the orientation of the ZnS films relative to the $Al_2O_3$-rod orientation. The stereogram of the point group 6mm, to which the ZnS belongs, is shown on the left, while that of the $\bar{3}m$ point group, to which the $Al_2O_3$ belongs, is shown on the right. The conventions used by Nye[6] are followed here. Heavy lines indicate mirror planes. The solid hexagon indicates a sixfold (hexad) axis of symmetry, while the open triangle indicates a threefold rotation axis plus a center of symmetry. $x_1x_2x_3$ and $X_1X_2X_3$ are the right-handed coordinate systems used for elastic and piezoelectric constant specification. $xyzu$ and $XYZU$ are the Miller-Bravais coordinate systems for hexagonal and trigonal symmetries.

The location of the $X_3$ or $c$ axis in the end face of the $Al_2O_3$ rod was determined by means of x-ray diffraction and marked on the cylindrical surface. Using reflection electron diffraction, the $x_1$ axis in each of the ZnS films was located and found to coincide with the $X_3$ axis of the $Al_2O_3$ substrate. The center section of Fig. 1 shows this relationship. The ZnS $x_3$ axis is parallel to the $Al_2O_3$ $X_1$ axis and the ZnS $x_1$ axis is parallel to the $Al_2O_3$ $X_3$ axis. CdS films deposited on another similarly oriented $Al_2O_3$ rod were found to have the same crystallographic orientation relative to the substrate as that described for the ZnS films.

## PHONON GENERATION

The piezoelectric matrix for hexagonal crystals of the 6mm class can be written thus

| | | $\epsilon_1$ | $\epsilon_2$ | $\epsilon_3$ | $\epsilon_4$ | $\epsilon_5$ | $\epsilon_6$ |
|---|---|---|---|---|---|---|---|
| | | $\sigma_1$ | $\sigma_2$ | $\sigma_3$ | $\sigma_4$ | $\sigma_5$ | $\sigma_6$ |
| $E_1$ | $P_1$ | · | · | · | · | $d_{15}$ | · |
| $E_2$ | $P_2$ | · | · | · | $d_{15}$ | · | · |
| $E_3$ | $P_3$ | $d_{31}$ | $d_{31}$ | $d_{33}$ | · | · | · |

The direct piezoelectric effect is defined in matrix notation by

$$P_i=d_{ij}\sigma_j \tag{1}$$

and the converse effect by

$$\epsilon_j=d_{ij}E_i, \tag{2}$$

where $i=1, 2, 3$ and $j=1, 2, \cdots, 6$. This matrix indicates that if a tensile stress $\sigma_3$ is applied parallel to the $x_3$ axis of the ZnS transducer, polarization will result along this axis alone, i.e.,

$$P_1=0, \quad P_2=0, \quad P_3=d_{33}\sigma_3 \tag{3}$$

or by the converse effect,

$$\epsilon_3=d_{33}E_3. \tag{4}$$

Hence, by applying an electric field perpendicular to the ZnS film, compressional waves alone will be generated at the transmitter end surface of the $Al_2O_3$ rod. The generated compressional waves propagate as plane waves[3] ($L$ mode) along the $Al_2O_3$ $X_1$ axis. On reaching the opposite end of the $Al_2O_3$ rod, the ZnS film is subjected to tensile stresses along its $x_3$ axis. The resultant polarization occurs along the $x_3$ axis alone as indicated by Eq. (4).

Referring to the piezoelectric matrix once more, it will be seen that a polarization along the $x_1$ axis of the ZnS film will be produced by a shear stress $\sigma_5$ about the $x_2$ axis, i.e.,

$$P_1=d_{15}\sigma_5, \quad P_2=0, \quad P_3=0 \tag{5}$$

or, by the converse effect,

$$\epsilon_5=d_{15}E_1, \quad \epsilon_1=\epsilon_2=\epsilon_3=\epsilon_4=\epsilon_6=0. \tag{6}$$

Similarly, a polarization along the $x_2$ axis of the ZnS film will be produced by a shear stress $\sigma_4$ about the $x_1$ axis, i.e.,

$$P_1=0, \quad P_2=d_{15}\sigma_4, \quad P_3=0 \tag{7}$$

or, by the converse effect,

$$\epsilon_4=d_{15}E_2, \quad \epsilon_1=\epsilon_2=\epsilon_3=\epsilon_5=\epsilon_6=0. \tag{8}$$

[4] J. de Klerk and E. F. Kelly, Appl. Phys. Letters **5**, 2 (1964).
[5] J. de Klerk and E. F. Kelly, Rev. Sci. Instr. **36**, 506 (1965).
[6] J. F. Nye, *Physical Properties of Crystals* (Oxford University Press, New York, 1960).

TABLE I. Attenuation and velocity characteristics.

| Mode in $Al_2O_3$ | Polarization (particle motion along axis) | Attenuation $\alpha_0$ dB/cm | Power law $n$ | Velocity (300°K) $\times 10^5$ cm/sec | | |
|---|---|---|---|---|---|---|
| | | | | This paper | Ref. 8 sample $SB1$ | Ref. 9 |
| $L$ Compressional | $X_1$ | 0.019 | 9 | 11.03 | 10.92 | 11.0 |
| $T_1$ Fast shear | $X_2$ | 0.036 | 7 | 6.78 | 6.69 | 8.9 |
| $T_2$ Slow shear | $X_3$ | 0.06 | 4 | 5.72 | 5.79 | 5.0 |

Hence by directing an electric field in the plane of the ZnS film along the $x_1$ axis, shear waves polarized along the $x_1$ axis of the ZnS film and along the $X_3$ axis of the $Al_2O_3$ will be generated. This mode will be referred to as the $T_2$ shear mode. By directing the electric field along the ZnS $x_2$ axis shear waves, polarized along the $x_2$ axis of the ZnS film and along the $X_2$ axis of the $Al_2O_3$, will be generated. This mode will be referred to as the $T_1$ shear mode. Both $T_1$ and $T_2$ modes propagate as pure shear modes[3] along the $X_1$ axis of the $Al_2O_3$.

## MEASUREMENT TECHNIQUE

The pulse-echo technique used for both attenuation and velocity measurements has been described in detail elsewhere.[7] Electric fields along the $x_3$ axes of the ZnS films were generated by using the disc metal electrodes shown in Fig. 12 of Ref. 7. For the generation of electric fields in the plane of the ZnS films along the $x_1$ or $x_2$ axes, the cavity shown in Fig. 2 of this paper was used. Two narrow parallel electrodes, rectangular in cross section, were used on opposite sides of the end faces of the $Al_2O_3$ rod. The arrangement of these electrodes is shown in Fig. 2. Figure 2(a) is a section in the plane containing the coaxial signal cables and the sample, whereas Figure 2(b) is a section taken at right angles to the plane of Fig. 2(a) and through one end of the sample. By rotating the sample between the electrodes the electric field can be directed along the $x_1$ or the $x_2$ axis of the ZnS film, or anywhere between these two axes. When directed along the $x_1$ axis, the electric field generates the $T_2$ shear mode and when directed along the $x_2$ axis, the $T_1$ shear mode is generated. In any intermediate direction in the $x_1x_2$ plane, the electric field has a component along both the $x_1$ and $x_2$ axes, resulting in the simultaneous generation of $T_1$ and $T_2$ modes.

## RESULTS OF THE MEASUREMENTS

The attenuation of each of the plane-wave modes along the $X_1$ axis of the $Al_2O_3$ rod was measured at 1 Gc/sec as a function of temperature. The velocities of the three modes were measured at room temperature alone. These values are given in Table I and compared with those measured by Wachtman *et al.*[8] and by J. Bhimasenachar.[9] The present measurements agree very well with those reported by Wachtman *et al.*, but differ markedly from those reported by Bhimasenachar. The present measurements and those reported by Wachtman *et al.* were conducted on optically clear synthetic $Al_2O_3$, whereas Bhimasenachar's measurements were conducted on a sample of naturally occurring corundum which was brown and opaque, and thus had a high concentration of impurities, which may have influenced the elastic constants and hence the acoustic velocities.

Also summarized in Table I are the values of $\alpha_0$ and $n$ given in Eq. (9) below. Figure 3 is a plot of the total attenuation $\alpha$ of each mode as a function of temperature, where

$$\alpha=\alpha_0+\alpha_1 T^n. \tag{9}$$

The temperature-independent value of attenuation at low temperature $\alpha_0$ was subtracted from the total attenuation and the difference $(\alpha-\alpha_0)$ plotted against temperature as the intrinsic attenuation $\alpha_I$ in Fig. 4.

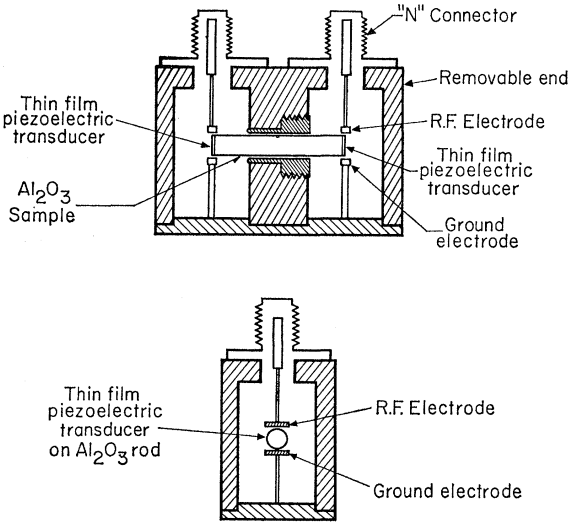


FIG. 2. Diagram showing electrode system used for shear-mode generation.

[7] J. de Klerk, Ultrasonics **2**, 137 (1964).

[8] J. B. Wachtman, Jr., W. E. Tefft, D. G. Lam, and R. P. Stinchfield, J. Res. Natl. Bur. Std. **64A**, 213 (1960).

[9] J. Bhimasenachar, Proc. Natl. Inst. Sci. India **16**, 241 (1950).

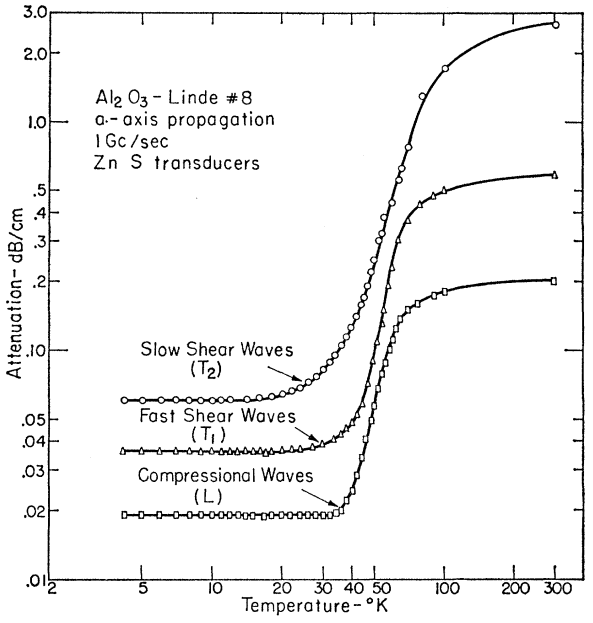


FIG. 3. Attenuation versus temperature for $Al_2O_3$, Linde No. 8.

Thus

$$\alpha_I=\alpha-\alpha_0=\alpha_1 T^n. \tag{10}$$

The value of $n$ was calculated from the slope of the $(\alpha_I-T)$ plots. Referring to these plots, it will be seen that while the $T_2$ mode has a single value of $n$ over the whole temperature range plotted, the $T_1$ and $L$ modes each have two distinct values of $n$, the breaks occurring between 50 and 60°K. In both cases the value of $n$, for temperatures above the knee, is the same as that for the $T_2$ mode, viz. four, whereas below the knees $n$ is greater than that for the $T_2$ mode, viz. seven and nine.

The total attenuation, plotted in Fig. 3, is included to indicate the effect of the acoustic quality of the sample. The value of $\alpha_0$, which is the sum of the acoustic losses due to the sample body and surface imperfections as well as those in the piezoelectric films, is a good indication of the sample quality. The lower the value of $\alpha_0$, the more accurately can the intrinsic attenuation, and hence the value of $n$, be determined.

Ciccarello *et al.*[1] reported a value of four for $n$ from measurements of compressional waves in ruby along the $c$ axis. An examination of the 0.5-kMc/sec curve of their Fig. 2 will show that a much better fit to the plotted points than their single $T^4$ curve would be achieved by using two straight lines of different slopes with the break in slope falling between 50 and 60°K. In fact, the suggested lines would pass directly through seven of the eight plotted points. An estimate of the two corresponding values of $n$ would approximate nine below 50°K and three above this temperature. Their 3-kMc/sec plot is a composite plot of measurements made on different samples with large temperature gaps and hence cannot yield an accurate estimate of $n$. The measurements of Fitzgerald and Truell, quoted by Ciccarello *et al.* in support of their claim to a $T^4$ dependence in ruby at 0.5 kMc/sec, have since been published.[2] Since the total attenuation changes by only 10% between 4 and 300°K, one cannot draw definite conclusions about the temperature dependence of $\alpha_I$ from it.

Referring to Fig. 4 of this paper, it will be seen that $\alpha_I$ for the compressional mode ($L$) at any chosen temperature is much lower than $\alpha_I$ for the slow shear mode ($T_2$). At 40°K, for example, the difference is greater than a factor 10. If the $\alpha_I$ plot for the $L$ mode is extrapolated to 25°K, then $\alpha_I$ would be more than 300 times smaller for the $L$ mode than for the $T_2$ mode.

## DISCUSSION

While the $T^4$ behavior of the $T_2$ mode is in rough agreement with the theory of Landau and Rumer,[10] the behavior of the other modes is not yet understood theoretically. If the mean free path of the thermal phonons is sufficiently long, the impressed wave is absorbed by anharmonic interactions between three phonons: an ultrasonic phonon and a thermal phonon combining to form another thermal phonon. Energy and momentum must be conserved, hence it can be shown that an ultrasonic wave can only interact with thermal waves which have a higher velocity. In this way we can see qualitatively why the $T_2$ wave, which can interact with thermal waves of the $T_1$ and the $L$ branch, has a higher anharmonic attenuation than the $T_1$ wave, which can only interact with thermal waves of the $L$ branch. One does not understand the $T^7$ behavior of the $T_1$ wave, nor the attenuation of the longitudinal wave.

The magnitude of the attenuation of the $T_2$ waves is in very rough agreement with the Landau-Rumer theory. The results of this theory may be expressed in the form[11]

$$\alpha=60\gamma^2(KT/Mv^2)(T/\Theta)^3(2\pi/\lambda), \tag{11}$$

where $\lambda$ is the wavelength of the impressed wave, $M$ is the average atomic mass, $v$ an average sound velocity, $K$ the Boltzmann constant, $\Theta$ the Debye temperature, and $\gamma$ the Grueneisen constant. Taking $\gamma=2$, $\Theta\simeq 1000$°K, and $v=7\times10^5$ cm$^{-1}$, so that $Mv^2/K=135\,000$°K, we obtain for the anharmonic attenuation at 30°K a value of $4.3\times10^{-3}$ cm$^{-1}$ or 0.019 dB/cm. This is in rough accord with the observed value of 0.03 dB/cm. In view of the approximations involved in deriving Eq. (11), in particular the uncertainty regarding the proper choice of $\gamma$, better agreement would be fortuitous.

[10] L. Landau and G. Rumer, Physik. Z. Sowjetunion **11**, 18 (1937).

[11] P. G. Klemens, *Physical Acoustics*, edited by W. P. Mason (Academic Press Inc., New York, 1965), Vol. 3B, Chap. 5.

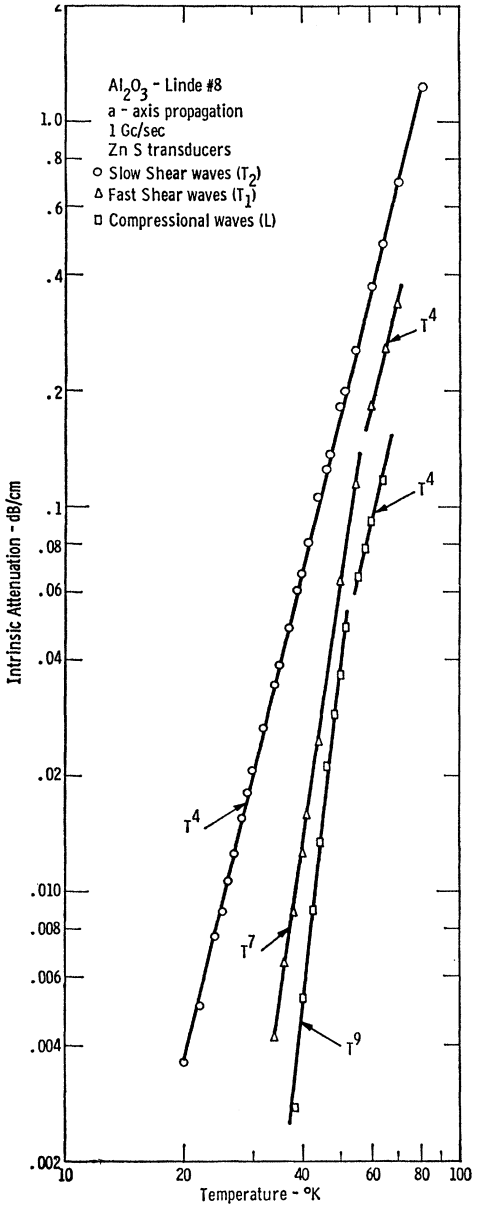


FIG. 4. Intrinsic attenuation versus temperature for $Al_2O_3$, Linde No. 8.

The attenuation of the longitudinal wave must be understood in terms of a partial relaxation of the momentum-conservation requirement in the three-phonon interaction, because the quantity $l/\lambda$ is no longer very large, where $l$ is the mean free path of the high-frequency thermal phonons interacting with the sound wave, and $\lambda$ the sound wavelength. This has been discussed by Maris.[12] The mean free path of the thermal phonons is limited by anharmonic interactions of the $N$ type, and may be estimated by extrapolating from the high-temperature thermal-conductivity data from the relation $l \propto \omega^{-2}T^{-3}$, where $\omega$ is the angular frequency of the thermal wave. Thus one would estimate that for the major component of thermal waves ($\omega \simeq 4KT/\hbar$), $l/\lambda \simeq 60$ at 30°K but only $\simeq 4$ at 50°K. Since $l$ decreases with increasing frequency, and since the rate of interaction due to the relaxation of the conservation conditions is proportional to $\lambda/l$, the major interaction occurs with waves of frequency of order $6\,KT/\hbar$ and is proportional to

$$T^9 \int [x^6 e^x/(e^x-1)^2]dx = T^9 J_6 \qquad (12)$$

instead of the normal $T^4 J_4$ dependence of the energy content. Since this proportionality holds only as long as $l/\lambda > 1$, one would expect deviations to occur at temperatures such that $l/\lambda \simeq 1$ at frequencies of order $6\,KT/\hbar$. At this point there should be significant deviations from the $T^9$ dependence. This may be the reason for the apparent break in the attenuation curve for the $L$ wave between 50 and 60°K. Note that at this point $l(\omega_1)/\lambda$ is still large, where $\omega_1 = KT/\hbar$, because of the frequency dependence of $l$.

In the case of the fast transverse wave there is an intermediate situation. This wave can still interact with longitudinal thermal waves, leading to a component of attenuation proportional to $T^4$, but less than that of the transverse waves by a factor of order $(1/v_L)^3 : (1/v_L)^3 + (1/v_{T_1})^3$, where $v_L$ and $v_{T_1}$ are the velocities of the longitudinal and the fast transverse waves. This factor is about 1:6. In addition, there should be a component due to interactions with thermal fast transverse waves, due to the relaxation of the momentum condition, again varying at $T^9$. The total attenuation is a combination of these two components.

## ACKNOWLEDGMENTS

The author would like to thank Dr. P. G. Klemens for his theoretical discussion of the measurements in the previous section, E. F. Kelly for depositing the piezoelectric thin-film transducers, T. P. Copan for determining the crystallographic orientation of the ZnS films, R. C. Kuznicki for the x-ray diffraction investigation, and F. N. Hauber for polishing the end faces of the $Al_2O_3$ rods.

[12] H. J. Maris, Phil. Mag. **91**, 901 (1964), who based his discussion on the work of S. Simons, Proc. Phys. Soc. (London) **82**, 401 (1963). See also the later work of S. Simons, Proc. Phys. Soc. (London) **83**, 749 (1964).